Shipping Container Impact Assessment for Tsunamis

Clay Naito, M.ASCE[1]; H.R. Riggs, M.ASCE[2]; Yong Wei[3,4], and Christina Cercone[5]

Abstract

During tsunami inundation coastal structures are subject to hydrostatic and hydrodynamic forces from the run up and run down and to impact forces from floating debris that is picked up by the flow. A new chapter in the upcoming revised U.S. design load standard covers these loads. To illustrate the application of this methodology for impact loading, it is applied to the determination of shipping container impact loads for locations in Hilo, Hawaii. The steps include: the identification of the tsunami design zone, the computation of the shipping container impact hazard region, and the computation of the design flow velocity and depth within that region. The flow velocity is used to determine the design impact force for the structure, and the depth is used to define up to what height impact must be considered. The standard provides a new, relatively simple 'energy grade line' (EGL) method that can be used to obtain estimates of these quantities. Because the method has not been widely validated within the archival literature, the results of the method are compared with results from a two-dimensional tsunami inundation simulation. A simple extension is proposed that can improve the results of the EGL. The paper is meant to provide a reference for those applying these provisions in practice, as well as to indicate areas for improvement.

Introduction

The on-shore flow during tsunamis transports a significant amount of debris. Larger debris, such as wood utility poles and logs, shipping containers, and marine vessels, can provide a significant impact force to on-shore structures during collision. Building codes and standards, if they consider debris impact events on structures as a result of tsunami and/or flooding, typically

[1] Corresponding Author, Associate Professor, Dept. of Civil and Environmental Engineering, Lehigh Univ., 13 E Packer Ave., Bethlehem, PA 18015, Email: cjn3@lehigh.edu
[2] Professor, Dept. of Civil and Environmental Engineering, Univ. of Hawaii, Honolulu, HI 96822
[3] Research Scientist, Joint Institute for the Study of Ocean and Atmosphere, Univ. of Washington, Seattle, WA 98105
[4] [4]Research Scientist, Pacific Marine Environmental Laboratory, National Oceanic and Atmospheric Administration, Seattle, WA 98115
[5] Graduate Student Researcher, Dept. of Civil and Environmental Engineering, Lehigh Univ., Bethlehem, PA 18015

suggest the application of procedures based on simple rigid body impact; see, e.g., ASCE (2010) and USACE (2006). Guidance on debris impact loads in ASCE 7-10 (ASCE 2010) is relegated to the commentary to that standard. Although that guidance is based on impulse-momentum for rigid body impact, it relies heavily on the experimental work by Haehnel and Daly (2002, 2004) on impact by woody debris. Recently, a significant amount of experimental and numerical research has been carried out on the impact forces related to tsunami debris such as poles, logs, and shipping containers (Yeom et al. 2009; Nouri et al. 2010; Madurapperuma and Wijeyewickrema 2012; Como and Mahmoud 2013; Piran Aghl et al. 2013; Naito et al. 2014; Piran Aghl et al. 2014a,b; Riggs et al. 2014; Ko et al. 2015; Piran Aghl et al. 2015). This later work has allowed the development of more physically-realistic models. The rigid body impact model appears to have been abandoned for the most part; the debris and, in some cases the structure, are treated as flexible.

An important aspect of debris impact is the probability of impact for a given site. Relatively little work has been done in this area. Some initial experimental studies have been undertaken to understand debris transport and dispersion onshore; see for examples, Rueben et al. (2011) and Yao et al. (2014). Some systematic work based on post-event surveys has also been carried out (Naito et al. 2014). However, the state-of-art is insufficient to quantify the risk of debris impact for a given site.

Currently, there is no U.S. national standard for either hydrodynamic loads or debris impact loads as a result of tsunamis. The American Society of Civil Engineers (ASCE) develops the U.S. design load standard ASCE 7, "Minimum Design Loads for Buildings and Other Structures" (ASCE 2010). The 2016 edition of the standard will include a new chapter on tsunami loading, which will apply to coastal regions of California, Oregon, Washington, Alaska and Hawaii. It includes hydrodynamic loads and debris impact loads, as well as effects such as scour. The debris impact loading provisions have been developed based on much of the previously mentioned recent research. Herein, reference to the 'standard' is to this new chapter of ASCE 7-16, and reference to the 'commentary' is to the commentary for this chapter. Although the standard is currently being published, many of the provisions in the standard have appeared elsewhere. Recent references are Chock (2015) and Carden et al. (2015), and an earlier reference is Chock (2012). A preliminary examination of the ASCE method for debris impact is presented in Riggs et al. (2015).

If a site is near a shipping container yard, the proposed ASCE 7 standard specifies a procedure to determine if impact by shipping containers, which can easily float if closed, must be considered in the structural design. While these provisions will affect a relatively small percentage of the overall buildings subject to tsunamis, the design impact loads can be quite large and they therefore may be significant for buildings that are affected. The procedure to determine the susceptibility to container impact involves a number of separate steps. While the steps are neither computationally nor theoretically difficult, they will be unfamiliar to most engineers faced with applying the standard. Furthermore, depending on the circumstances, engineering judgment may be required to obtain the design loads, especially in regards to determining the design flow depth and velocity. An understanding of the source of the provisions, the reasons for the assumptions, and the general methodology used to obtain the background data will enhance the quality of these judgments. This paper is meant to contribute to this understanding.

The tsunami loading provisions do not apply to all buildings. The standard defines four Tsunami Risk Categories, which are the risk categories defined in the existing standard with some modifications. The tsunami loading provisions apply to Tsunami Risk Categories III and IV, and, when required by the local building code, to a few (tall) buildings in category II. It is assumed herein that the target building is in a risk category that requires tsunami loads to be considered. In that case, the following steps are required to apply the tsunami provisions for a given building site:

1. Determine if the site is subject to flooding from tsunami
2. Determine the maximum flow depth and flow velocity at the site
3. If the site is near a discrete source of debris, such as a shipping container yard, determine the debris impact zone of the debris source and determine if the site is in the zone
4. Use the flow velocity and depth to calculate the design impact loads and the locations at which those loads must be applied

In the next several sections, each of these steps is illustrated. To demonstrate the application of the provisions, they are applied to the vicinity of a container yard at Hilo Harbor, Hawaii. However, the approaches and discussion are kept general and therefore will be of interest to practicing engineers faced with applying the standard to other regions. The determination of the maximum design flow depth and flow velocity is key to obtaining the design impact forces. One approach to obtain these is through a site-specific inundation analysis. However, the standard allows the use in many cases of a much simpler method. That method is used herein to demonstrate its use, and the results are compared with values from a site-specific analysis to determine its performance for the Hilo region in the context of impact loading. A straightforward modification of the method is proposed to improve the results.

The methodology reported herein will be applied by practicing engineers, and a major objective is to illustrate its application. One unique aspect of the present work is that rather than consider a single building site, the impact forces at a number of locations are determined. This allows contour lines of impact force to be drawn for the impact zone of the container yard. While this is more work than application to a single site, it might be useful in practice for site selection purposes and for urban planning.

Tsunami Design Zone

Based on site-specific tsunami inundation modeling for the maximum considered tsunami for a given locale, ASCE has produced maps that show the extent of inundation (inland extent of the water flow) for much of the populated coasts of the five affected states. If an area does not have an inundation map, the standard specifies a procedure to estimate the runup based on the offshore wave height, which is provided for all locations. In addition, it is anticipated that state and local jurisdictions will produce additional inundation maps. The area between the shore and the inundation limit is defined as the Tsunami Design Zone (TDZ). The ASCE inundation data (area of inundation and runup data along the inundation limit) will be available on an ASCE website (the ASCE website is not public at the time of writing). The first step is to obtain from this site the kmz file (keyhole markup language zipped) that shows the TDZ for the specific area. Figure 1 depicts the TDZ for Hilo using Google Earth (Google 2015) (Although this TDZ is based on the final ASCE inundation modeling, the TDZ illustrated in this paper is preliminary and minor details may exist between it and the final TDZ). Due to the topography and the characteristics of the inundation, dry pockets are present in the TDZ. It is a simple matter to determine if a given building site is in the TDZ. The kmz file also contains the longitude, latitude, and simulated tsunami runup height (i.e., the water elevation relative to a specified datum) for discretized points along the inundation limit; see Figure 2. These data are required input to the procedure to obtain the water depth and flow velocity within the TDZ, as explained subsequently.

Maximum Flow Depth and Maximum Velocity

Assuming the building site is in the TDZ, the next step is to determine the maximum design flow depth and flow velocity for the site. If the maximum flow depth is less than 0.914 m (3 ft), the standard does not require debris impact to be considered. The rationale for this is that many important types of debris will interact significantly with the ground in smaller water depths, and that because of the already small flow velocities, impact forces are expected to be relatively small. At greater flow depths it is assumed that debris will move at the flow velocity. The standard allows two approaches to determine the maximum design flow depth and maximum design flow velocity.

The first approach is a site-specific inundation analysis. Such an analysis requires at least a depth-integrated two-dimensional model for the fluid flow. There are several software packages available to do these analyses, such as MOST/ComMIT (Titov et al. 2011), COULWAVE (Lynett et al. 2002), COMCOT (Liu et al., 1995), GeoClaw (LeVeque and George 2008), and NEOWAVE (Yamazaki et al. 2011). However, it is the authors' opinion that these analyses should be carried out only by specialists experienced in tsunami inundation modeling.

For most structures, the standard does not mandate the use of a site-specific inundation analysis. Instead, it allows use of a simplified 'Energy Grade Line Analysis', which computationally is a straightforward calculation procedure that can be done easily in, for example, a spreadsheet program and that can be carried out in a typical structural design office. Even when a site-specific analysis is used, an energy grade line (EGL) analysis is also required because the velocities from a site specific analysis cannot be used to reduce the design values below a specified percent of those from an EGL analysis.

Prior to calculating the depth and velocity, an elevation map of the region is required.

Digital Elevation Model (DEM)

Although Google Earth is convenient to view the TDZ and the inundation line, the ground elevations in Google Earth are not necessarily sufficiently accurate for calculations. More accurate digital elevation data can be obtained from the National Oceanic and Atmospheric Administration (NOAA) National Centers for Environmental Information (NCEI) (NOAA 2015). The metadata associated with the dataset will specify the resolution. For many areas, a cell size of 1/3 arc sec, i.e. approximately 10 m (33 ft), will be available. The data is provided in the format of a 'matrix' of elevation values referenced to a vertical datum of Mean High Water (MHW), North America Vertical Datum of 1988 (NAVD88), or Mean Sea Level (MSL). The metadata specify the datum as well as the latitude and longitude of the bottom left cell. The coordinates of the other data points are obtained by incrementing the starting coordinates with the cell size (e.g., 1/3 arc sec). These data can be viewed in a variety of software tools, including ArcGIS (ESRI 2015) and Matlab (MathWorks 2015). The DEM data for the specific building site, including the region from the coast to the inundation limit, can be combined with ASCE's digital runup data from step 1.

Figure 3a, which was created using Matlab, shows for Hilo the topography based on the NOAA DEM data (Love et al. 2011), referenced to MHW, and the ASCE inundation limit. Note that the ASCE inundation data consists of discrete data points consisting of latitude, longitude, and runup elevation. It should be noted that the runup points from Figure 2 were used to produce a more functional inundation line in Figure 3.

The ASCE runup heights are referenced to the vertical datum of MHW and NAVD88 for coastal regions of Washington, Oregon, and California. Because the NAVD88 datum is not available in Alaska and Hawaii, the runup heights in coastal regions of these two states are referenced to MHW. To use the ASCE runup elevations, one should ensure that the elevations are relative to the same datum as used for the DEM datum.

Reconciling DEM data and runup elevation

There can be a mismatch between the DEM elevation and the runup elevation; that is, the elevation for given latitude and longitude in the DEM data may not match the ASCE runup elevation for the same point. There are several reasons for this. First, the DEM data that a user has obtained per the previous section may differ from the DEM data that was used for the runup modeling. For Hilo, the topographic data in the Hilo DEM used for the ASCE inundation simulations were obtained from the National Geospatial-Intelligence Agency (NGA) Hawaii Interferometric Synthetic Aperture Radar (IfSAR). The IfSAR dataset is more accurate than the

United States Geological Survey (USGS) 1/3-arc-sec National Elevation Dataset (NED) available to the general public through the NCEI. Love et al. (2011) reported that the IfSAR data has a vertical accuracy of 2 m or better in areas of unobstructed ground. This vertical accuracy is poorer than topographic lidar (0.14 to 0.2 m) but much greater than the USGS NED 1/3-arc-sec data, which may have as poor as 7 to 15 m vertical accuracy (Love et al., 2011). In situations where the DEM data used for the ASCE runup simulations are not available, one should use the ASCE inundation limit together with the most accurate DEM data that is available.

A comparison of the DEMs using IfSAR and USGS NED topography is presented in Figure 3. The DEM using the IfSAR topography (Figure 3a) provides a greater level of accuracy than the one using the USGS NED topography (Figure 3b). The errors in elevation between the two DEMs are illustrated in Figure 3c. As illustrated the elevation errors for this region occur primarily outside of the tsunami design zone. The sensitivity of results to the difference in DEMs will be investigated subsequently.

To understand the second reason for possible discrepancies, one must understand how the runup data are obtained. The runup modeling is two-dimensional using a grid in the horizontal *x*-*y* plane, and each cell (element) is given a constant elevation. The grid size used for the ASCE runup simulations was 2 arc sec (~ 60 m). If the DEM data are at 1/3 arc sec (~ 10 m), then there are 36 DEM cells per runup modeling element, and the runup element uses an average elevation. Therefore, it is possible for the runup elevation (the sum of the element elevation and the calculated water depth) to be either larger or smaller than the DEM elevation for a given point. Figure 4 illustrates a hypothetical situation where the ground profile is increasing in elevation from left to right. The 'DEM data' is shown as discrete points on the ground profile. Programs will typically interpolate linearly when queried for the elevation between defined DEM data points. Clearly, the ground elevation of a point corresponding to the last 'wet' element can be either below the calculated water elevation or above it. Even if the same data and same grid spacing were to be used, there could be a mismatch because the modeling software can only calculate a finite water depth; that is, it will never calculate a water elevation that will equal the elevation of the element. Indeed, the runup model used to compute the ASCE TDZ considers the cell to be 'dry' when the water depth in that cell is less than 0.1 m.

The standard assumes the water depth at the inundation limit is zero. However, it should be obtained by subtracting the DEM ground elevation from the ASCE runup elevation. The situation when the runup elevation is significantly higher than the ground elevation is discussed subsequently.

Flow transect

The next step to determine the maximum depth and velocity is to establish a flow transect from the shoreline, through the building site, to the inundation limit. The basic approach is to establish a point on shore where a line parallel to the shore, averaged over 304 m (1,000 ft), i.e., ±152 m (±500 ft) on either side, has a normal that passes through the building site. Consider building site A in Figure 5. The line "Flow Transect" illustrates an appropriate transect for this site (the same transect could be used for any building site that falls on the line). This transect then needs to be rotated ±22.5º about the building site (site A), to obtain a 'cone' that extends from the building site to the inundation line. The design flow conditions may be obtained from the transect within this cone that results in the most conservative conditions. As explained in the commentary of ASCE 7-16, the requirement to consider this 45° arc reflects both some variability in the flow direction, and hence the direction of force, as well as a desire to obtain conservative design values.

There can be several challenges to determining the appropriate transect for certain practical conditions. The most easily identifiable transect normal to the shore going through Site B intersects the inundation line before reaching the site, and a different transect must be chosen. Site C has multiple potential transects. One possibility is to use the closest coast normal; however, engineering judgment would need to be used, applying an understanding of the likely direction of flow. The standard also allows a site-specific analysis to be used. If one is carried out, then it can be used to determine the direction of flow and an appropriate transect can be chosen.

Once the flow transect has been determined, the distance from the shore to the inundation limit, x_R, is determined. Also, the ground elevations along the transect with a maximum horizontal spacing of 30.5 m (100 ft) must be determined from the inundation limit to the building site (or possibly the shore). The result is a set of points (x, z), with the x–coordinate increasing in the direction from shore to the inundation limit (i.e., directed inland) and z is directed upwards. For subsequent computation, it is convenient if the first point is at the inundation limit and the last point is at the building site. Also, along the transect appropriate values for Manning's coefficient must be chosen. The standard provides common values for different surfaces, ranging from open land to urban development. Other values from the literature can be used, e.g., Bunya et al. (2010). It should be noted that it is fairly common for the runup modeling to be based on a uniform value of 0.03, which is close to 'bare earth'. However, the commentary states that the inherent conservatism designed into the EGL analysis typically would not require the use of a value above 0.05. (As will become clear, using larger values of Manning's coefficient results in larger design depths and velocities in the EGL analysis.)

Once x_R, the points (x, z), the runup depth h_R, and the Manning's coefficients have been determined, an EGL analysis can be used to obtain the maximum flow depth and velocity at the building site.

Energy Grade Line Analysis

The EGL analysis defined in the standard is a somewhat ad hoc method to use the inundation and runup from a site-specific probabilistic tsunami hazard analysis to obtain the design flow depth and design flow velocity at a building site. It is a simplified engineering tool to make tractable for many design situations a problem that would otherwise require sophisticated numerical modeling. It has been developed to provide statistically conservative results, at least for the maximum momentum flux that is used for the hydraulic loading. The development and validation of the method is presented in Kriebel et al. (2016), with some initial tuning of the method carried out by Wiebe (2013) using FUNWAVE-TVD (Shi et al. 2011). The method has been based on a very large number of simulations for essentially idealized topographies. It is therefore important to evaluate the method for real-world scenarios. Comparisons with field measurements during the Tohoku tsunami indicated that the method provided conservative values for the sites considered (Carden et al., 2015). Given that it is the velocities that are used for impact, detailed comparisons between the EGL results and a site-specific analysis are made herein to contribute to the continuing evaluation of the EGL method.

The EGL analysis is based on the concept of an energy grade line for steady, one-dimensional flow. Because tsunami flow is not steady, some ad hoc modifications are required, as introduced subsequently. The coordinate along the transect, x, is assumed to increase from shore to the inundation limit. For steady, one-dimensional flow, the energy equation can be written as

$$\frac{dE_g}{dx} = -(\phi + s) \tag{1}$$

in which the head above ground elevation is $E_g = h + u^2/2g$, with h = flow depth and u = flow velocity; $\phi = dz/dx$ is the ground slope, and $s = u^2 / [(k/n)^2 h^{4/3}]$ is the standard Manning formulation for frictional losses. The parameter n is the Manning coefficient and k is 1.0 for SI units and 1.49 for US customary units.

The standard uses a (forward) Euler approach to solve Eq. (1). Such an approach results in a simple recursive relation to calculate E_g, if the calculation is started at a location where E_g, h and u are known. The only location where these are known in advance is at the inundation limit, where u is assumed to be zero. It should be noted that the standard assumes h is (essentially) zero at the inundation limit. However, as discussed previously, the ASCE runup height may be larger than the ground elevation at the inundation limit. As shown subsequently herein, it is better to modify the procedure to obtain more conservative results in such cases. The commentary to the standard suggests using a small nominal depth (0.03 m or 0.1 ft) at the inundation limit. This was chosen to avoid a problem with s when $h = 0$, but a cleaner solution, used herein, is to set $s = 0$ whenever $h = 0$.

Because the initial conditions at the inundation limit are known, the standard cleverly reverses the direction of evaluation, going from the inundation limit towards shore, and the relation becomes

$$E_{g,i+1} = E_{g,i} + (\phi_i + s_i) \cdot \Delta x_i \tag{2}$$

where $E_{g,i}$ and s_i are evaluated based on h_i and u_i, $\Delta x_i = x_i - x_{i+1}$, and $\phi_i = (z_i - z_{i+1})/\Delta x_i$. The index i is 1 at the inundation limit and increases toward the building site. The change in sign between Eqs. (1) and (2) is because the latter equation progresses in the $-x$ direction. The calculation can also be extended to the shore if the velocity and flow depth at the shore are desired.

It should be noted that one can also proceed from shore to the inundation limit. In that case, however, one must iterate on the flow depth at the shore to obtain the specified flow depth at the inundation limit (or at whichever target point is used).

Eq. (2) involves both h and u. For steady flow, the continuity equation for steady flow is used to provide a second relation. However, this can't be used in the case of unsteady tsunami flow, and therefore the standard assumes a relation between the two variables. Specifically, it is assumed that the Froude number, $Fr = u\big/\sqrt{gh}$, varies from a maximum value, α, at the shore to zero at the inundation limit via

$$Fr = \alpha\left(1 - \frac{x}{x_R}\right)^{1/2} \quad (3)$$

The square root relation in Eq. (3) was taken as a result of the investigation by Wiebe (2013). The parameter α is the Froude number at the shore. The standard allows this to be taken as 1.0 unless it is known that the tsunami hits the shore as a bore, in which case a value of 1.3 is to be used. The standard provides guidance on the conditions that might result in a bore. See Carden et al. (2015) for justification of the 1.3 value. Eq. (3) allows the Froude number to be determined for all points prior to evaluating Eq. (2). Although the standard distinguishes between tsunamis that hit the shore as bores or not to calculate the velocity, the debris impact scenario assumes that the impact is post-bore, i.e., it does not consider explicitly debris contained in the bore front.

It is now straightforward to formulate Eq. (2) as an explicit algebraic equation in the single unknown h_{i+1}:

$$h_{i+1} = \frac{h_i\left(1+0.5Fr_i^2\right)+(\phi_i+s_i)\Delta x_i}{1+0.5Fr_{i+1}^2} \quad (4)$$

The calculation can be stopped once the building site is reached; there is no need to continue to the shore. Given the maximum design depth, the maximum design velocity is readily calculated from the Froude number. However, the standard states that the maximum design velocity cannot be taken smaller than 3.0 m/s (10 ft/s) and it need not be taken greater than 15.2 m/s (50 ft/s).

In some cases, the transect may intersect an elevated portion of land that has a higher elevation than the runup point. The standard requires the runup point to be at least equal to the highest elevation along the transect. Therefore, the elevation of the runup point must be raised artificially to equal the highest elevation along the transect. This was done in Figure 6, which shows the result of the EGL analysis for the flow transect at Site A. Note that the zero location for this site corresponds to the building site, not the shore.

Performance and Modifications of EGL Analysis

The EGL approach is compared with the results of the ASCE site specific analyses for the three transects at each site (A, B and C) identified in Figure 5. The site-specific inundation analyses were carried out with the tsunami model MOST (Method of Splitting Tsunamis) (Titov and Gonzalez 1997; Titov and Synolakis 1998). The maximum velocity and maximum inundation depth at the site from the site specific analyses are given in Table 1; note that the maximum depth and maximum velocity do not occur simultaneously. The results from the EGL analyses for the three transects at each site are also shown. The most likely scenario will be to use the values from the transect with the maximum momentum flux to define the inundation at the site, as compared to using different values for different directions. These results are noted in bold in the table. As illustrated, the difference in the transect path and topography can result in a considerable variation in estimated inundation for a given site. The EGL method underestimated the site specific inundation at all but one site and underestimates the velocity at all sites. Part of the underestimation can be attributed to the fact that the velocity and inundation height at the run up is assumed to be zero in the EGL analysis, when in reality this may not be the case. Utilizing the known inundation elevation at the run up line, which is provided as part of the available TDZ data, a modified approach to the EGL analysis is proposed here to account for the fact that the inundation at the run up point may not be zero.

Extended EGL Analysis

The modified EGL analysis, referred to as the Extended EGL, involves extending the transect past the run up to a point where the ground elevation is equal to the runup height at the inundation limit. The EGL analysis is then performed following the same procedure outlined previously from the extended EGL end point to the site. Extending the EGL results a non-zero inundation elevation at the run up as well as a non-zero velocity at this location.

The EGL and extended EGL are compared in Figure 6 for site A and in Table 1 for sites A, B, and C. The extended EGL transects are also illustrated in Figure 5. Note that due to the ground topography and the water depth at the run up the extension can in some cases be very long (see transect C1) or very short (see transect B2). Because the length of the transect is extended and the starting elevation is higher, the velocity and inundation increase. This is clear from the comparison of the EGL and extended EGL for the flow transect at site A (Figure 6). As

Table 1 reveals, the Extended EGL results in a conservative estimate of the inundation depth at all three sites. While the corresponding velocities also increase significantly, they are still underpredicted, in this case by an average of 16%. Based on these comparisons the extended EGL method is recommended.

Sensitivity of EGL Analysis to DEM

The sensitivity of the EGL results to variations in DEMs is examined using the IfSAR and USGS DEM ground elevation data. The results of the Extended EGL method are compared to the site specific analyses. The extended EGL was run for each of the three transects from site A. The velocity and inundation depth and ground elevation from the site to the extended run up are shown in Figure 7. Because the site specific data are based on the IfSAR data, but at a reduced sampling resolution as discussed above, these two elevations are comparable. The elevations between the USGS and IfSAR data show some differences, most notably for the +22.5 and Center transects beyond the inundation limit. The EGL estimates of velocity and inundation are similar for both DEMs. Depending on the differences in topography, in some cases the IfSAR data result in higher values and in other cases lower. Based on this comparison the difference in DEMs would not result in considerable differences in estimated demands. That is, the method appears to be relatively stable with respect to small differences in elevation models.

Recommended Flow Depth and Velocity for Design

For steady flow, the depth and velocity from the energy approach occur at the same time, but this is not the situation for a tsunami. It is assumed that the depth and velocity determined by the EGL analysis are the maximum values over all time, but clearly in a tsunami these maxima do not occur simultaneously. Based on video analysis after the Tohoku tsunami (Ngo and Robertson, 2012) as well as numerical simulations, the standard assumes a phase-shifted variation of these two quantities. Based on this variation, the standard specifies three Load Cases. Load Case 1 is meant primarily to check building buoyancy effects on initial arrival of the tsunami. Although there are some cases where it might govern for impact, it is building-specific and will not be considered herein. In Load Case 2, the maximum velocity obtained in the EGL analysis is assumed to occur with a flow depth equal to 2/3 the maximum depth computed in the EGL analysis. In Load Case 3, the velocity is taken to be 1/3 the maximum from the EGL analysis with the maximum flow depth.

As mentioned, if the maximum flow depth at the building site is less than 0.914 m (3 ft), then the standard does not require one to consider debris impact. Otherwise, the container impact hazard region must be determined to ascertain whether or not the building site is within this region.

Container Impact Hazard Region

The procedure to define the tsunami hazard zone was based on the post-Tohoku analysis of the displacement of containers and boats documented in Naito et al. (2014). A second EGL analysis is required to determine the container impact hazard region. In this case, the 'building site' in the previous section is taken to be the container yard. That is, the transect goes from shore, through the center of the yard, to the inundation limit; see Figure 8. The depths along this transect are calculated as above. The nominal container impact hazard region extends from the container yard along the transect until a depth of 0.914 m (3 ft) is reached. As before, a 45º cone is drawn, with a vertex at the container yard. Multiple transects in this cone can be evaluated to determine the extent of the inflow hazard region based on this depth criterion. In this case, the minimum flow depth is reached very close to the inundation limit; see Figure 8.

The inflow hazard region can be terminated prior to the 0.914 m (3 ft) water depth based on the 'density' of the dispersed shipping containers. An estimate of the total plan areas of all the shipping containers likely to be at the container yard is made. This area is then distributed across the land area until the cone has an average 'container density' (container plan area to ground area) of 2%. If the extent of this area is less than the depth limit, the extent of the hazard region can be curtailed.

As noted previously, relatively little work has been done on tsunami debris dispersion, especially in a quantitative sense that can then be applied to structural design. There is no "model" available. The method in the standard is based on relatively limited data from one event, the 2011 Tohoku tsunami (Naito et al. 2014). Therefore, application of this hazard region specification requires engineering judgement. If an engineer has reason to believe that the hazard region should be expanded, then that should be done. The standard specifies minimum design loads.

For the Hilo example illustrated in Figure 8, the authors estimate a worst case of 514 – 6.2 m

(20 ft) and 1,418 – 12.2 m (40 ft) standard shipping containers at the container yard. With an average density of 2%, this equates to a 45º arc with a radius of 2.52 km (8,260 ft). For this case the 2% arc exceeds the runup line and therefore this criterion is not effective at this location and the limit of 0.914 m (3 ft) governs the extent of the impact hazard region.

The extent of the hazard area can also be curtailed if there are structural steel and/or concrete structures inland of the yard that are deemed to form an effective barrier to dispersal of the containers. The height of these structures must be at least the calculated water depth minus 0.61 m (2 ft). If there is more than 0.61 m (2 ft) of water over the structures, then it is assumed the containers can float over them. The Hilo area provides no such barrier.

Once the inflow hazard region is determined, the cone is 'flipped' so that the vertex is now at the inland extent of the region, which in this case is the 0.914 m (3 ft) inundation depth along the central transect. This cone is extended to the shore to define the outflow hazard region; see Figure 8. The union of these two areas defines the container impact hazard region. If the building site is in the inflow (outflow) region only, it need be designed only for impact on the shore (leeward) side of the structure. If it is in both regions, it must be designed for impact in both directions.

Impact Force and Duration

In lieu of further analysis, the standard allows a conservative prescriptive design load of 955 kN (214.5 kips) to be used. This load should be multiplied by the importance factor, which is 1.0 for Tsunami Risk Category II buildings and 1.25 for Tsunami Risk Category III and IV buildings. The Tsunami Risk Categories are based on ASCE 7 Risk Categories with minor modifications for tsunami effects. In the following, all forces are computed based on an importance factor of 1.0.

The standard specifies equations to obtain a design load that may be smaller than above. The equation for the nominal instantaneous impact force, F_{ni}, is

$$F_{ni} = u\sqrt{km_d} \tag{5}$$

in which u is the flow velocity, k is most often the container stiffness, and m_d is the mass of the empty container. The standard provides values of k for 6.1 m (20 ft) and 12.2 m (40 ft) containers: 42.9 MN/m (245 kip/in) and 29.8 MN/m (170 kip/in), respectively. The corresponding values for empty mass (weight) are 2,270 kg (5,000 lb) and 3,810 kg (8,400 lb). The flow speed is used as a conservative estimate, based on the assumption that the container has had sufficient time to obtain that speed, and has not been hindered by interaction with the ground or other obstacles. The maximum value of F_{ni} is obtained by using the maximum flow speed at the site calculated in the EGL analysis. In any event, the value of F_{ni} need not be taken larger than 980 kN (220 kips). Interestingly, for 6.1 m (20 ft) and 12.2 m (40 ft) containers, Eq. 5 results in the limiting force being reached at 3.1 m/s (10.2 ft/s) and 2.88 m/s (9.45 ft/s), respectively. Therefore, the limit will almost always be reached, although there is still an advantage of doing the calculations because of the different load cases. In addition, the stiffness k in Eq. 5 is actually to be the lessor of the container stiffness and the stiffness of the structural member being impacted, such as a column or a wall. Therefore, it is possible to obtain smaller impact forces if the stiffness of the structural member is smaller than the container stiffness.

The structural member can be impacted in a flexural mode or in a shear mode. The flexural column stiffness associated with a mid-height impact is illustrated in Figure 9. The flexural member stiffness for fixed-fixed, simple-simple, and simple-fixed boundary conditions are illustrated and compared to the recommended container stiffness of 42.9 MN/m (245 kip/in) and 29.8 MN/m (170 kip/in) for the 6.1 m (20 ft) and 12.2 m (40 ft) shipping containers under longitudinal impact. The column stiffness are expressed as functions of the shear stiffness EI/L^3, where E is the elastic modulus, I is the gross moment of inertia, and L is the span. Hence, Figure 9 can be used for any generic column. For example, to determine the stiffness to use in Eq. 5 for impact of a 12.2 m (40 ft) container on a 457 mm (18 in) square concrete column, the EI/L^3 value would need to be computed. If the column is 6.10 m (20 ft) long with an elastic modulus of 25.2 GPa (3650 ksi), the EI/L^3 would be 405 kN/m (2.31 kip/in). For a simple-simple boundary condition, the structural stiffness of the component would control and the stiffness would be 19.3 MN/m (110 kip/in). However, for simple-fixed or fixed-fixed boundary conditions, the container stiffness would control and the stiffness would be limited to 29.8 MN/m (170 kip/in). For a shear dominated impact (i.e., one near the support) the shear stiffness of the structural member would exceed the container stiffness for most common elements. For example the shear stiffness for an impact point load on a 457 mm (18 in) square concrete column located one column depth from the support would be 5,040 MN/m (28,800 kip/in).

Eq. 5 gives the nominal maximum instantaneous impact force. The design instantaneous impact force, F_i, is obtained from F_{ni} by multiplying by two factors (in addition to the importance factor discussed above). The equation for F_{ni} is based on a conservative head-on impact scenario. To reflect that the impact will most probably be at an oblique angle, which would result in a lower force, F_{ni} is multiplied by an orientation coefficient of 0.65. For example, this drops the 980 kN (220 kip) force to 637 kN (143 k).

The second factor relates to the dynamics of impact. A typical design approach is to apply the force statically, and therefore a dynamic response factor, R_{max}, must be applied. R_{max} depends on the ratio of the duration of impact to the natural period of the structural member being impacted. The duration of impact is taken as

$$t_d = \frac{2m_d u_{\max}}{F_{ni}} \tag{6}$$

for an empty container and

$$t_d = \frac{\left(m_d + m_{contents}\right)u_{\max}}{F_{ni}} \tag{7}$$

for a loaded container. $m_{contents}$ is assumed to be 50% of the maximum rated content capacity of the container, and values are given in the standard. Based on these two durations, the maximum dynamic response factor is selected to obtain F_i. The dynamic response factor is essentially the same as specified in ASCE 7-10 in the flood commentary (ASCE 2010). It has a minimum value of 0 for a duration of 0, has a peak of 1.8, and levels off at 1.5 for impact durations that are long relative to the natural period of the structural member. Because R_{max} depends on the structural member's period, the forces presented subsequently do not include this factor (i.e., they are for a factor of 1.0).

Results of EGL Analysis for Hilo

A debris source consisting of a container yard is identified at coordinates (19.7303°,–155.0536°). The geometry of the yard is demarked using imagery from Google Earth as illustrated in Figure 2. The geometric center of the yard is identified and used as the vertex for the inflow hazard region as previously illustrated in Figure 8.

For illustration purposes the inundation depth and maximum flow velocity were calculated over the entire container impact hazard region. An EGL analysis was conducted over the region every 0.001° longitude and latitude, which corresponds to a grid spacing of approximately 110 m (360 ft). The maximum inundation depths and velocities are illustrated as contour plots in Figure 10. From the velocity data the design instantaneous debris impact force can be computed. Herein the force generated from a 6.1 m (20 ft) container is illustrated. As noted previously due to the requirement that the minimum inundation velocity be 3.05 m/s (10 ft/s) and that the maximum impact force may be limited to 637 kN (143 kip), load case 2 results in the 637 kN (143 kip) demand over the container impact region where inundation depth exceeds 0.914 m (3 ft). For load case 3 the velocities are reduced to 1/3 and therefore the maximum force is only achieved for sites near the coast (Figure 11).

Conclusions

The 2016 edition of the ASCE 7 Load Standard details an approach to determine design forces generated by impact of tsunami borne debris. The approach consists of the identification of the tsunami design zone, determination of a debris site within the tsunami design zone, computation of impact hazard region from the debris site, and the computation of the design flow velocity and depth using the EGL method. The flow depth is used to determine if debris can travel to the building site as well as the height of impact loads. The flow velocity is used to determine the design impact load for the structure. The paper provides a case study that illustrates the methodology for Hilo, Hawaii. In addition to demonstrating the procedures for practicing engineers, a modification of the EGL method is proposed for when the ASCE-provided inundation depth at the inundation limit is not zero. In addition, results indicate that the EGL results may not be overly sensitive to reasonably small variations in the DEM. The paper should be of interest to practicing engineers faced with applying the new methodology.

The standard represents a first attempt to provide design engineers with appropriate loads to design for container impact. The standard uses a combination of state-of-the-art methodology (e.g., the site specific inundation analysis) and practical, simplified approaches (e.g., the energy grade line method). There are a number of areas in which improvements can be made. First, the inundation simulation tools have been validated primarily in terms of inundation and runup; Although studies have been carried out to validate nearshore flow velocities (Arcas and Wei, 2011; Yamazaki et al., 2012; Arcos and LeVeque, 2014; Admire et al., 2014; Zhou et al., 2014), additional validation is needed for the flow velocities based on field measurements in the flooding zone. The EGL method should be developed further, including validating or improving the assumption of the variation of Froude number and considering more complicated scenarios than straight transects. The impact force equation is based principally on either a rigid structure or a rigid debris; this can be improved; see Khowitar et al. (2014, 2015) for improved formulations. The authors anticipate that the 2022 edition of ASCE 7 will have some of these, and other, improvements.

Acknowledgements

The authors would like to recognize the efforts of the ASCE 7 Tsunami Loads and Effects Subcommittee, which has developed a comprehensive standard for design loads for structures subject to tsunami effects. The committee was chaired by Gary Chock, S.E., F.SEI, F.ASCE, D.CE., and the subcommittee's work was funded by ASCE. The authors would like to express their appreciation to Gary Chock for helpful discussions related to this paper. The authors also express their appreciation to Prof. David Kreibel for discussions on the EGL method.

Yong Wei's work is funded by the Joint Institute for the Study of the Atmosphere and Ocean (JISAO) under NOAA Cooperative Agreement NA10OAR430148, Contribution No. 2430, PMEL Contribution No. 4322.

References

Admire, A.R., Dengler, L.A., Crawford, G.B., Uslu, B.U., Borrero, J.C., Greer, S.D., and Wilson, R. (2014). "Observed and modeled currents from the Tohoku-oki, Japan and other recent tsunamis in northern California." *Pure Appl. Geophys*., 171, 3385-3403.

Arcas, D, and Y. Wei (2011): Evaluation of velocity-related approximations in the non-linear shallow water equations for the Kuril Islands, 2006 tsunami event at Honolulu, Hawaii. *Geophys. Res. Lett.*, *38*, L12608, doi: 10.1029/2011GL047083, 6 pp.

Arcos, M.E.M. and LeVeque, R.J. (2014). "Validating velocities in the GeoClaw tsunami model using observations near Hawaii from the 2011 Tohoku tsunami", *Pure Appl. Geophys.*, 172, 849-867.

ASCE (2010). "Minimum design loads for buildings and other structures." ASCE/SEI 7-10, American Society of Civil Engineers.

Bunya, S., Dietrich, J. C., Westerink, J. J., Ebersole, B. A., Smith, J. M., Atkinson, J. H., Jensen, R., Resio, D. T., Luettich, R. A., Dawson, C., Cardone, V. J., Cox, A. T., Powell, M. D., Westerink, H. J., and Roberts, H. J. (2010). "A High-Resolution Coupled Riverine Flow, Tide, Wind, Wind Wave, and Storm Surge Model for Southern Louisiana and Mississippi. Part I: Model Development and Validation." *Monthly Weather Review,* 138(2), 10.1175/2009mwr2906.1, 345-377.

Carden, L., Chock, G., Yu, G., and Robertson, I. (2015). "The New ASCE Tsunami Design Standard Applied to Mitigate Tohoku Tsunami Building Structural Failure Mechanisms." *Handbook of Coastal Disaster Mitigation for Engineers and Planners*, Butterworth Heinemann, 461-490.

Chock, G. (2012). 'ASCE 7 and the development of a tsunami building code for the U.S." 14th U.S.-Japan Workshop on the Improvement of Structural Design and Construction Practices, Wailea-Makena, HI, ATC, 6-1 - 6-11.

Chock, G. (2015). "The ASCE 7 Tsunami Loads and Effects Design Standard for the United States." *Handbook of Coastal Disaster Mititgation for Engineers and Planners*, M. Esteban, H. Takagi, and T. Shibayama, eds., Butterworth Heinemann, 437-460.

Como, A. and Mahmoud, H. (2013). "Numerical evaluation of tsunami debris impact loading on wooden structural walls." *Engineering Structures,* 56, 10.1016/j.engstruct.2013.06.023, 1249-1261.

ESRI (2015). "ArcGIS." http://www.arcgis.com/features/. (March 30, 2015).

Google (2015). "Google Earth." http://www.google.com/earth/. (March 30, 2015).

Haehnel, R. B. and Daly, S. F. (2002). "Maximum impact force of woody debris on floodplain structures." ERDC/CRREL TR-02-2, US Army Corp of Engineers, Engineer Reserach and Development Center.

Haehnel, R. B. and Daly, S. F. (2004). "Maximum impact force of woody debris on floodplain structures." *Journal of Hydraulic Engineering*, 130(2), 112-120.

Khowitar, E., Riggs, H. R., and Kobayashi, M. H. (2014). "Beam response to longitudinal impact by a pole." *Journal of Engineering Mechanics*, 140(7), 10.1061/(ASCE)EM.1943-7889.0000765, 04014045.

Khowitar, E., Riggs, H. R., and Kobayashi, M. H. (2015). "Transverse impact of a horizontal beam on a vertical column." *Journal of Engineering Mechanics*, 10.1061/(ASCE)EM.1943-7889.0001011, 04015085.

Ko, H. T.-S., Cox, D. T., Riggs, H. R., and Naito, C. J. (2015). "Hydraulic experiments on impact forces from tsunami-driven debris." *Journal of Waterway, Port, Coastal, and Ocean Engineering,* 141(3), 10.1061/(ASCE)WW.1943-5460.0000286, 04014043.

Kriebel, D., Lynett, P. J., Cox, D. T., Petroff, C. M., Robertson, I. N., and Chock, G. Y. K. (2016). "Energy method for approximating overland tsunami flows." *Journal of Waterway, Port, Coastal and Ocean Engineering*, under review.

Lebreton, L. C. and Borrero, J. C. (2013). "Modeling the transport and accumulation floating debris generated by the 11 March 2011 Tohoku tsunami." *Mar Pollut Bull*, 66(1-2), 10.1016/j.marpolbul.2012.11.013, 53-58.

LeVeque, R. J. and George, D. L. (2008) High-resolution finite volume methods for the shallowwater equations with bathymetry and dry states. In P. L. Liu, C. Synolakis, and H. Yeh, editors, Advanced Numerical Models for Simulating Tsunami Waves and Runup, volume 10 of Advances in Coastal and Ocean Engineering, pages 43-73. World Scientific.

Liu, P. L.-F., Cho, Y.-S., Briggs, M. J., Kanoglu, U., and Synolakis, C. E. (1995). ''Runup of solitary waves on a circular island.'' *J. Fluid Mech.*, 302, 259–285.

Love, M. R., Friday, D. Z., Grothe, P. R., Lim, E., Carignan, K. S., Eakins, B. W., and Taylor, L. A. (2011). "Digital elevation model of Hilo, Hawaii: procedures, data sources and analysis." NOAA National Geophysical Data Center, Boulder, Colorado.

Lynett, P., Wu, T.-R., and Liu, P. L.-F. (2002) "Modeling Wave Runup with Depth-Integrated Equations," *Coastal Engineering*, v. 46(2), p. 89-107.

Madurapperuma, M. A. K. M. and Wijeyewickrema, A. C. (2012). "Performance of Reinforced Concrete Columns Impacted by Water-Borne Shipping Containers." *Advances in Structural Engineering,* 15(8), 1307-1327.

MathWorks (2015). "MATLAB The Language of Technical Computing." http://www.mathworks.com. (March 30, 2015).

Naito, C., Cercone, C., Riggs, H. R., and Cox, D. (2014). "Procedure for site assessment of the potential for tsunami debris impact." *Journal of Waterway, Port, Coastal, and Ocean*

Engineering, 140(2), 10.1061/(ASCE)WW.1943-5460.0000222, 223-232.

Ngo, N. and Robertson, I. N. (2012). "Video Analysis of the March 2011 Tsunami in Japan's Coastal Cities." UHM/CEE/12-11, University of Hawaii, Honolulu.

NOAA (2015). "National Centers for Environmental Information (NCEI)." http://www.ncei.noaa.gov/. (September 4, 2015).

Nouri, Y., Nistor, I., Palermo, D., and Cornett, A. (2010). "Experimental investigation of tsunami impact on free standing structures." *Coastal Engineering Journal,* 52(1), 10.1142/S0578563410002117, 43-70.

Piran Aghl, P., Naito, C. J., and Riggs, H. R. (2013). "An experimental study of demands resulting from in-air impact of debris." *Satefy, Reliability, Risk and Life-Cycle Performance of Structures and Infrastructures*, G. Deodatis, B. R. Ellingwood, and D. M. Frangopol, eds., Taylor and Francis Group, London, 5541-5547.

Piran Aghl, P., Naito, C., and Riggs, H. R. (2014a). "Full-scale experimental study of impact demands resulting from high mass, low velocity debris." *Journal of Structural Engineering,* 140(5), 10.1061/(ASCE)ST.1943-541X.0000948, 04014006.

Piran Aghl, P., Naito, C. J., and Riggs, H. R. (2014b). "Estimation of demands resulting from inelastic axial impact of steel debris." *Engineering Structures,* 82(1), 10.1016/j.engstruct.2014.10.021, 11-21.

Piran Aghl, P., Naito, C. J., and Riggs, H. R. (2015). "A simplified model for estimating axial impact forces resulting from debris with nonstructural mass." *Structural Engineering and Mechanics,* in review.

Riggs, H. R., Cox, D. T., Naito, C. J., Kobayashi, M. H., Piran Aghl, P., Ko, H. T.-S., and Khowitar, E. (2014). "Experimental and analytical study of water-driven debris impact forces on structures." *Journal of Offshore Mechanics and Arctic Engineering,* 136, doi:10.1115/1.4028338, 041603.

Riggs, H. R., Naito, C. J., Cercone, C., and Wei, Y. (2015). 'ASCE 7 Structural Load Provisions for Impact by Tsunami-driven Shipping Containers." Coastal Structures & Solutions to Coastal Disasters Joint Conference, Boston, MA, ASCE, 11 pp.

Rueben, M., Cox, D., Holman, R., Shin, S., and Stanley, J. (2015). "Optical measurements of tsunami inundation and debris movement in a large-scale wave basin." *Journal of Waterway, Port, Coastal and Ocean Engineering*, 141(1), 10.1061/(ASCE)WW.1943-5460.0000267, 04014029.

Shi, F., Kirby, J. T., Tehranirad, B., and Harris, J. C. (2011). “FUNWAVE-TVD, documentation and users' manual.”University of Delaware, Newark, DE.

Titov, V. V. and Gonzalez, F. I. (1997). “Implementation and testing of the Method of Splitting Tsunami (MOST) model.” NOAA Technical Memorandum ERL PMEL-112 (PB98-122773), NOAA/Pacific Marine Environmental Laboratory, Seattle, WA.

Titov, V. V., Moore, C. W., Greenslade, D. J. M., Pattiaratchi, C., Badal, R., Synolakis, C. E., and Kânoğlu, U. (2011). “A New Tool for Inundation Modeling: Community Modeling Interface for Tsunamis (ComMIT).” *Pure and Applied Geophysics,* 168(11), 10.1007/s00024-011-0292-4, 2121-2131.

Titov, V. V. and Synolakis, C. E. (1998). “Numerical modeling of tidal wave runup.” *Journal of Waterway, Port, Coastal and Ocean Engineering,* 124(4), 157-171.

USACE (2006). ‘Coastal Engineering Manual.” U.S. Army Corps of Engineers.

Yamazaki, Y., Cheung, K.F., Pawlak, G. and Lay, T. (2012). "Surge along the Honolulu coast from the 2011 Tohoku tsunami." *Geophys. Res. Lett.*, 39, L09604, doi:10.1029/2012GL051624.

Yamazaki, Y., Cheung, K.F., and Kowalik, Z. (2011). Depth-integrated, non-hydrostatic model with grid nesting for tsunami generation, propagation, and run-up. *International Journal for Numerical Methods in Fluids*, 67(12), 2081-2107.

Yao, Y., Huang, Z., Lo, E. Y. M., and Shen, H.-T. (2014). “A Preliminary Laboratory Study of Motion of Floating Debris Generated by Solitary Waves Running up a Beach.” *Journal of Earthquake and Tsunami*, 08(03), 10.1142/s1793431114400065, 1440006.

Yeom, G.-S., Nakamura, T., and Mizutani, N. (2009). “Collision analysis of container drifted by runup tsunami using drift collision coupled model.” *Journal of Disaster Research,* 4(6), 441-449.

Wiebe, D. M. (2013). “Tsunami Inundation: Estimating Damage and Predicting Flow Properties.” MS thesis, Oregon State University, Corvallis, Oregon, USA, 102 pp.

Zhou, H., Y. Wei, L. Wright, and V. Titov (2014). “Waves and currents in Hawaiian waters induced by the dispersive 2011 Tohoku tsunami”. *Pure Appl. Geophys.*, 171(12), doi: 10.1007/s00024-014-0781-3, 3365-3384.

List of Figure Captions

Figure 1. Tsunami Design Zone for Hilo (Data MBARI, Data SOEST/UHM, Image © 2015 DigitalGlobe)

Figure 2. Points of runup height along the inundation limit for Hilo (Data MBARI, Data SOEST/UHM, Image © 2015 DigitalGlobe)

Figure 3. Digital elevation models for Hilo region (a) DEM topographic data and runup for the Hilo area using USGS NED topography, (b) DEM using NGA IfSAR topography, (c) Elevation difference in feet between the DEM using NGA IfSAR and USGS NED topography

Figure 4. Discrepancy between models

Figure 5. Transects from shore

Figure 6. Comparison of EGL and Extended EGL for flow transect at site A.

Figure 7. Comparison of DEMs with site specific data at Site A

Figure 8. Container Impact Hazard Region (adapted from Riggs et al. 2015)

Figure 9. Stiffness of structural component based on mid-height impact

Figure 10. Maximum inundation depth (a) and flow velocity (b) in container impact hazard region

Figure 11. Design instantaneous debris impact force for 6.1 m (20 ft) containers in hazard region for Load Case 2 (a) and Load Case 3 (b)

Tables

Table 1: Comparison of EGL, extended EGL and site specific analyses

Site	Transect	Inundation Depth [m (ft)]			Velocity [m/s (ft/s)]		
		EGL	Extended EGL	Site Specific	EGL	Extended EGL	Site Specific
A	(-) 22.5	**6.19(20.31)**	7.03(23.08)	7.70(25.27)	**5.98(19.61)**	6.48(21.26)	7.59(24.89)
A	Center	5.75 (18.88)	**10.23(33.57)**		5.48(17.97)	**7.52(24.67)**	
A	(+) 22.5	3.61(11.83)	9.05(29.68)		4.22(13.86)	6.81(22.33)	
B	1	0.62(2.03)	3.05(10.00)	2.62(8.61)	0.75(2.45)	2.26(7.42)	2.93(9.60)
B	2	0.41(1.36)	1.66(5.44)		0.59(1.93)	1.21(3.97)	
B	3	**0.81(2.66)**	**3.25(10.67)**		**1.03(3.38)**	**2.25(7.38)**	
C	1	1.26(4.12)	**10.19(33.43)**	7.68(25.19)	2.43(7.97)	**8.55(28.04)**	11.31(37.12)
C	2	6.73(22.07)	8.76(28.74)		7.05(23.14)	8.17(26.80)	
C	3	**8.12(26.63)**	9.36(30.70)		**7.85(25.74)**	8.46(27.76)	

Figure 1. Tsunami Design Zone for Hilo (Data MBARI, Data SOEST/UHM, Image © 2015 DigitalGlobe)

Figure 2. Points of runup height along the inundation limit for Hilo
(Data MBARI, Data SOEST/UHM, Image © 2015 DigitalGlobe)

Figure 3(a) DEM topographic data and runup for the Hilo area using USGS NED topography

Click here to download Figure Figure3a.tif

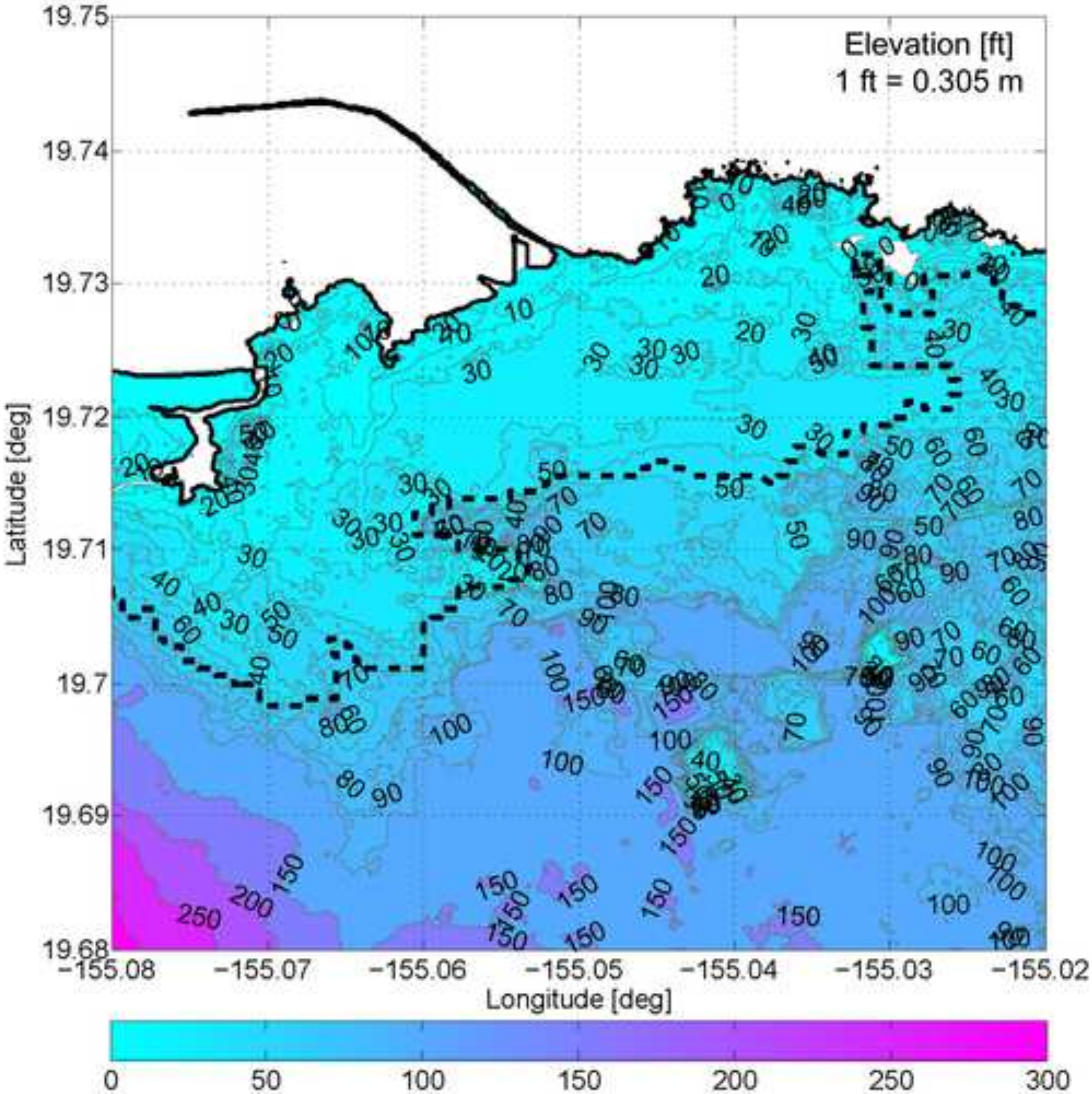

Figure 3(b) DEM using NGA IfSAR topography

Click here to download Figure Figure3b.tif

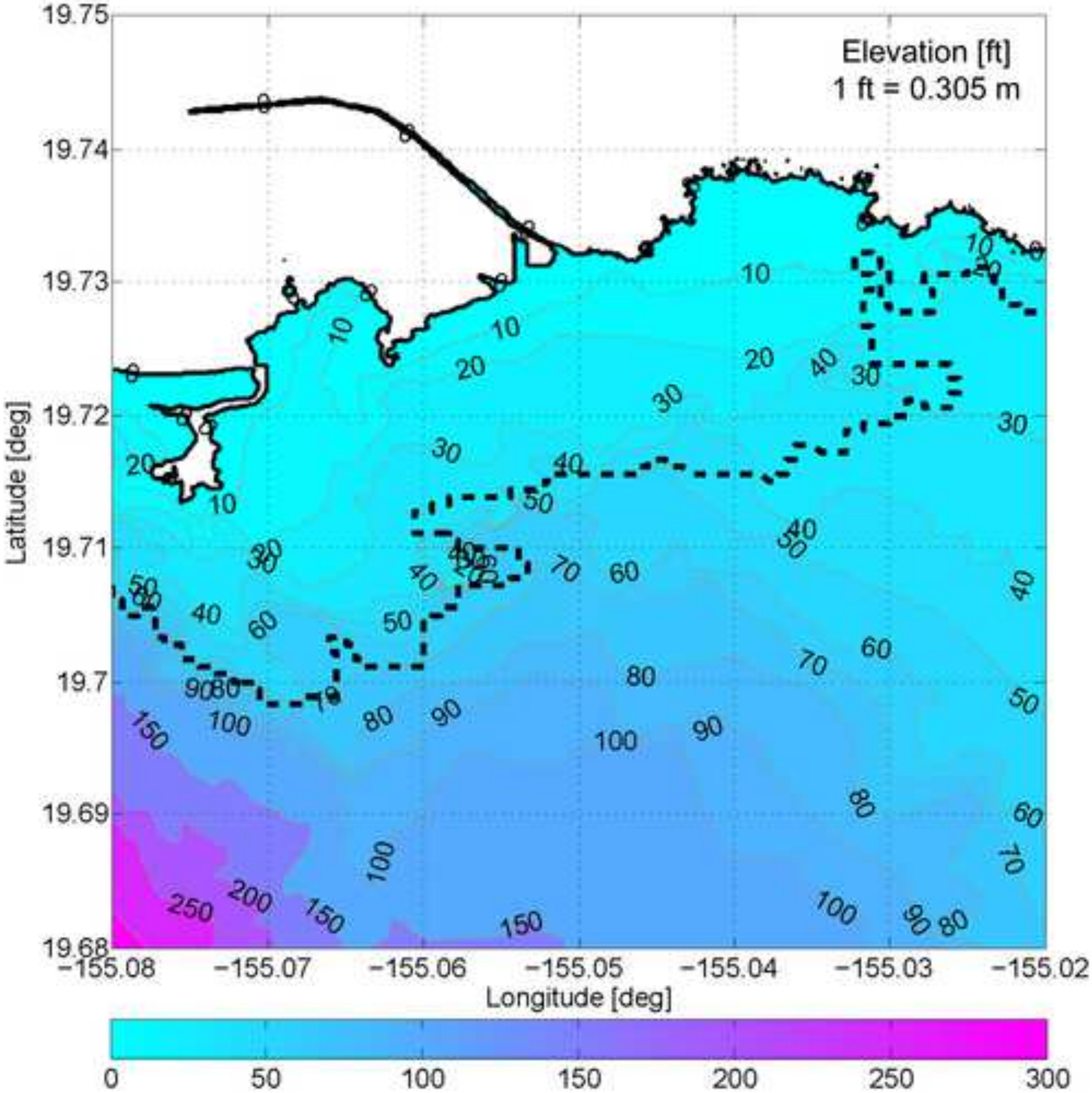

Figure 3(c) Elevation difference in feet between the DEM using NGA IfSAR and USGS NED topography

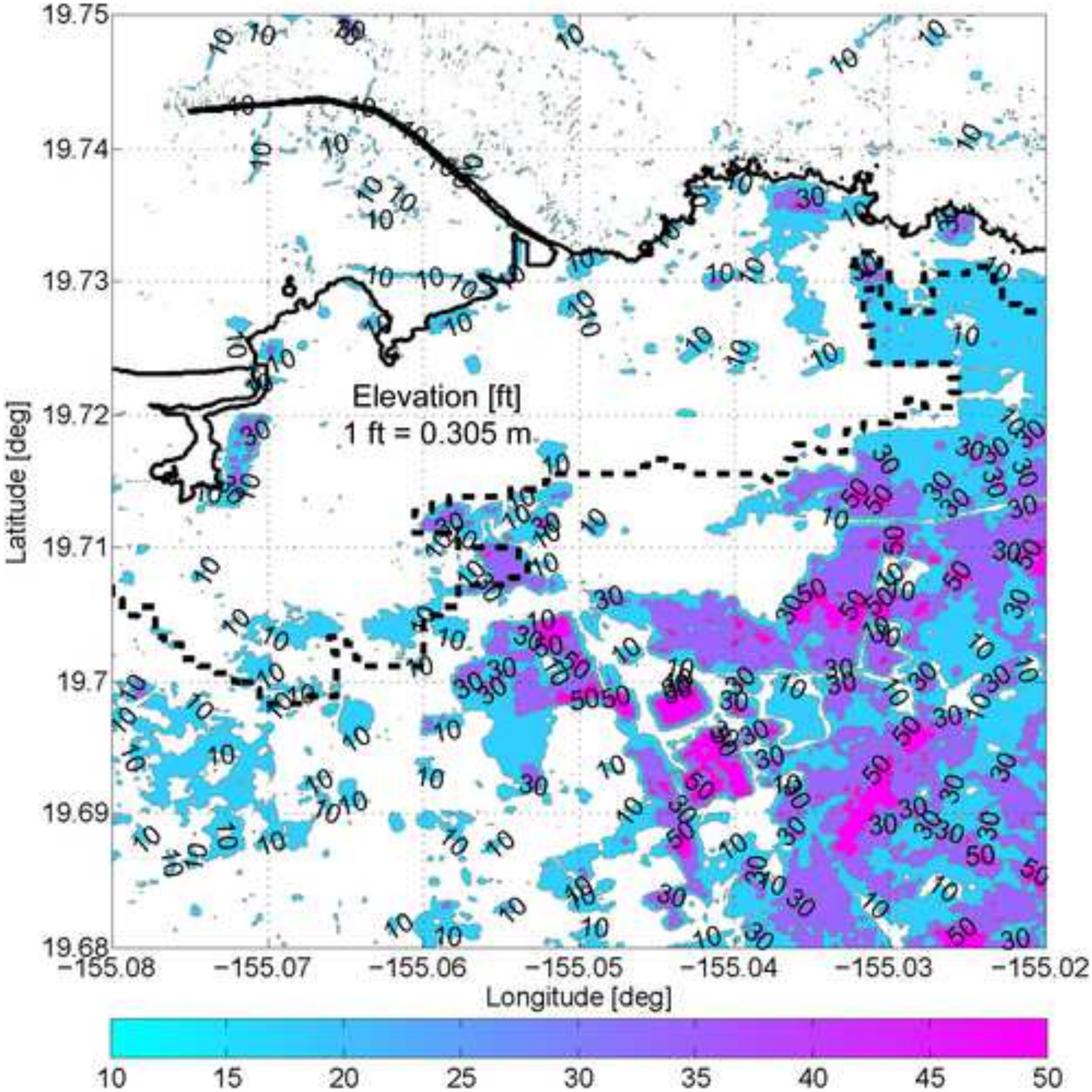

Figure 4. Discrepancy between models

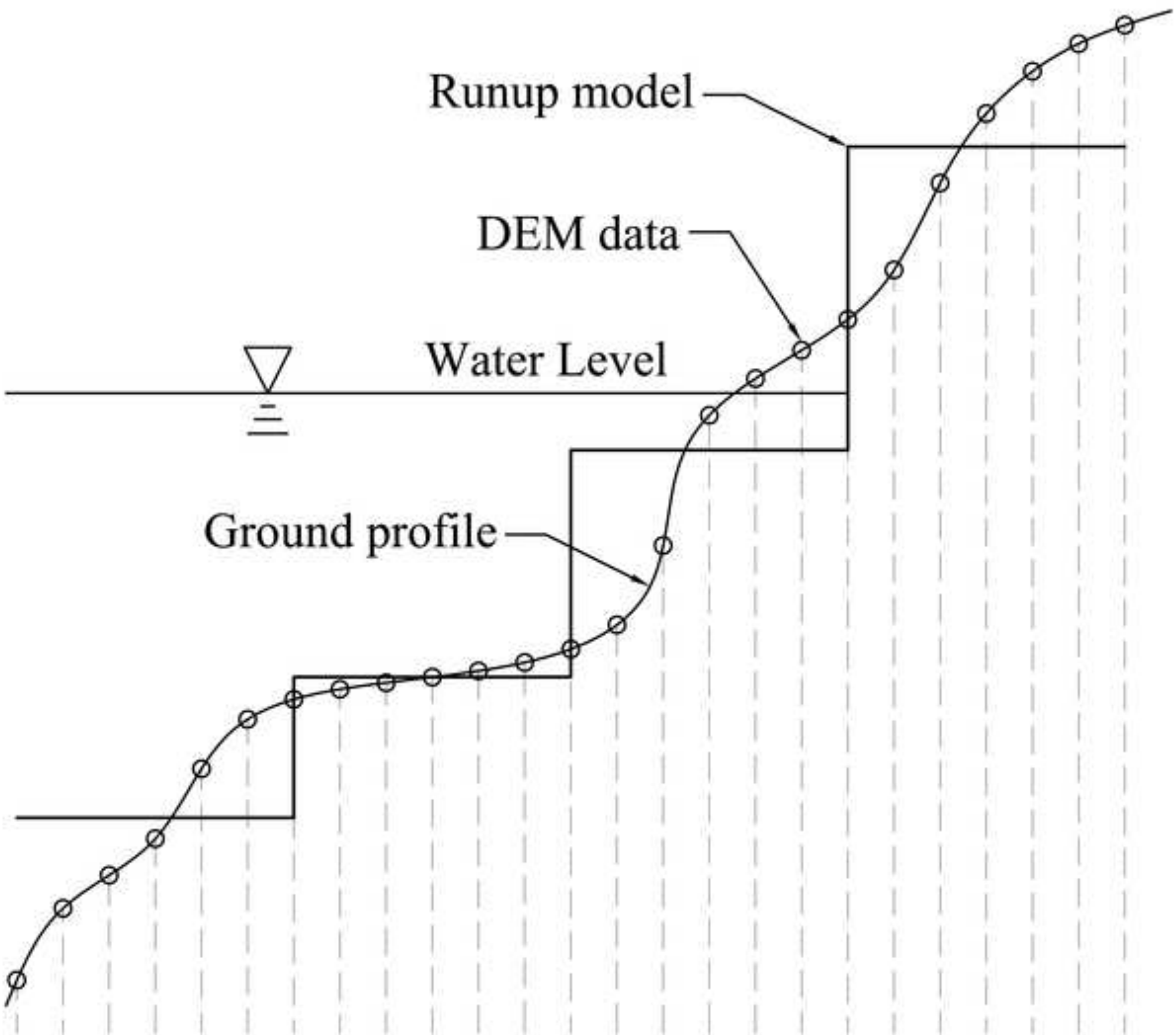

Figure 5. Transects from shore

Click here to download Figure Figure5.tif

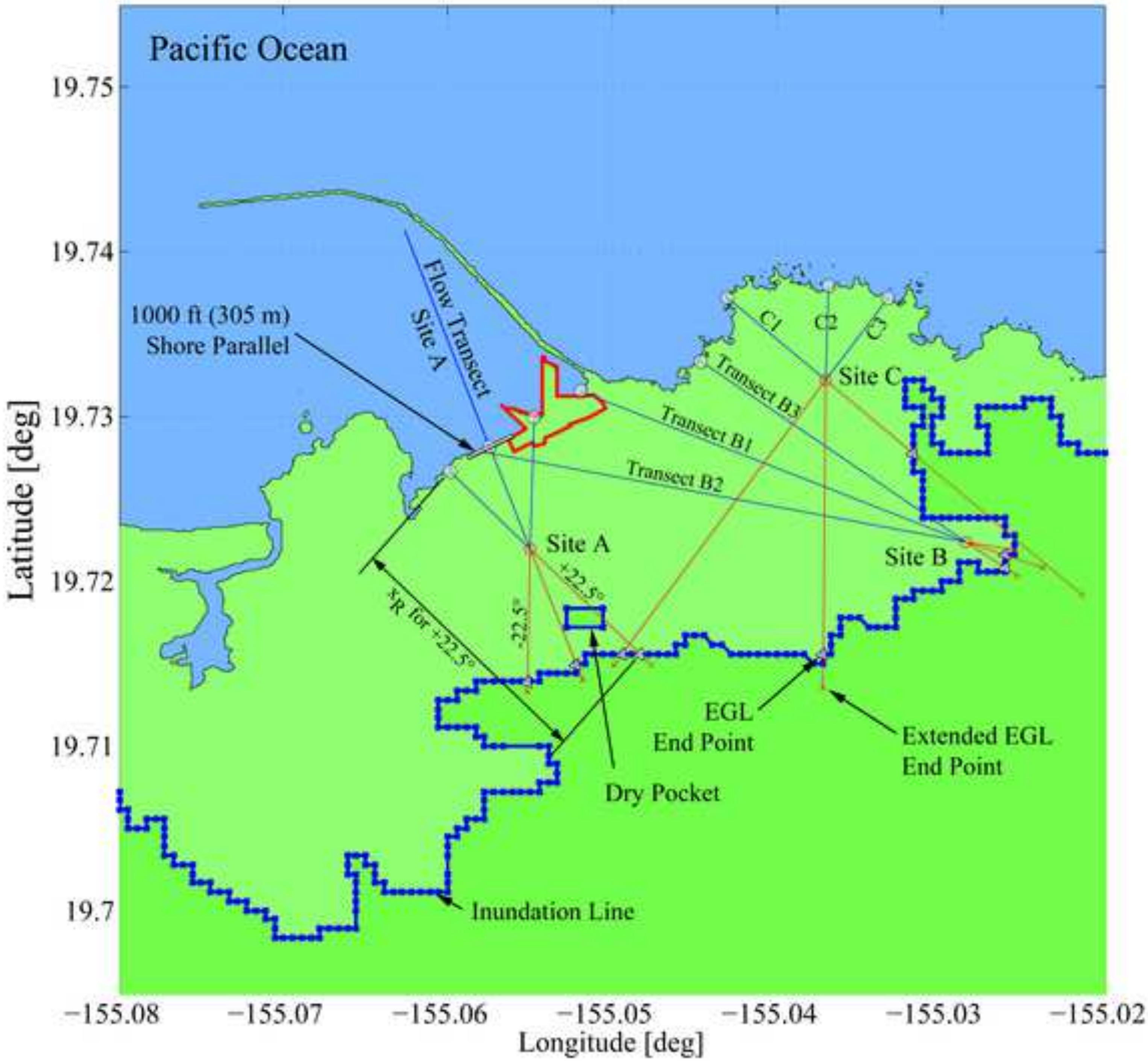

Figure 6. Comparison of EGL and Extended EGL for flow transect at site A

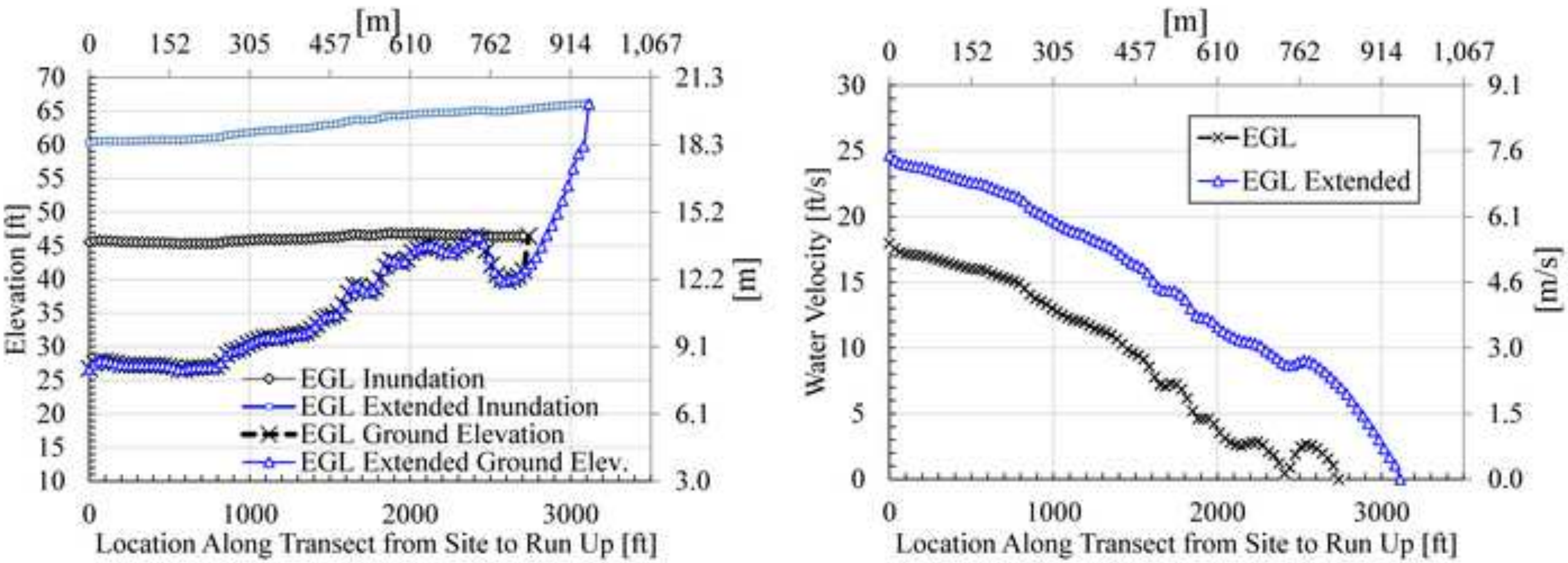

Figure 7. Comparison of DEMs with site specific data at Site A

Click here to download Figure Figure7-new.tif

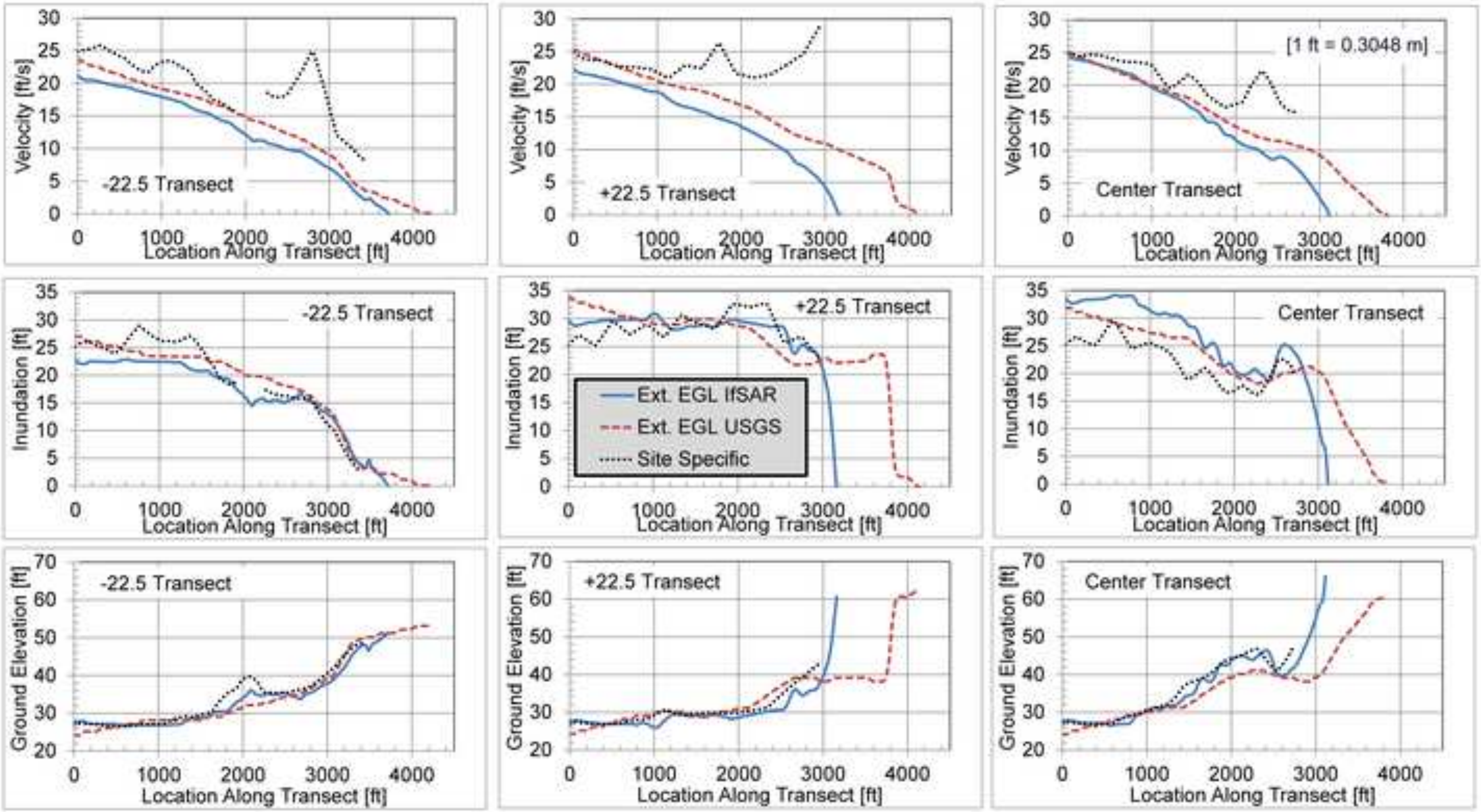

Figure 8. Container Impact Hazard Region (adapted from Riggs et al. 2015)

Click here to download Figure Figure8.tif

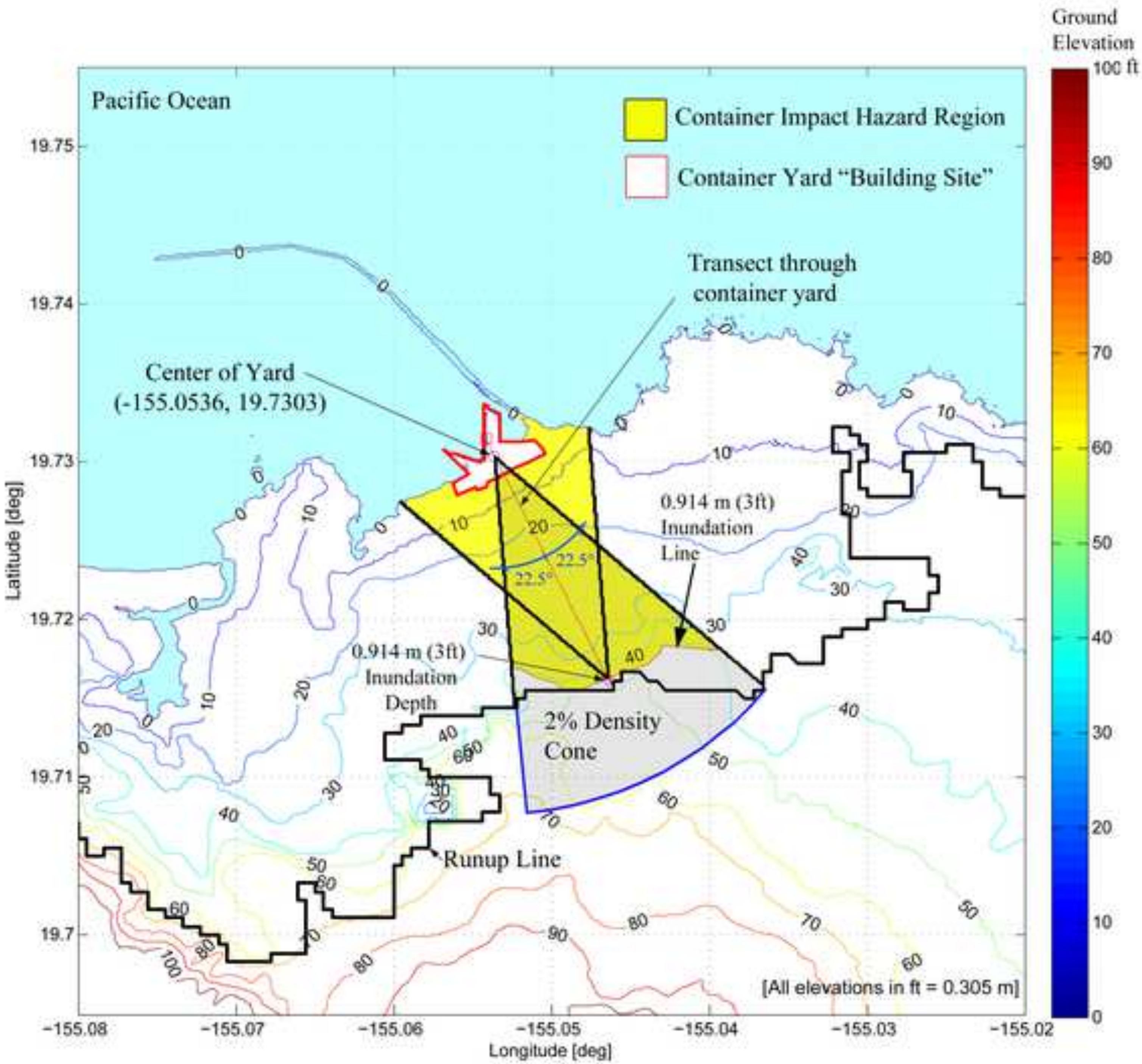

Figure 9. Stiffness of structural component based on mid-height impact

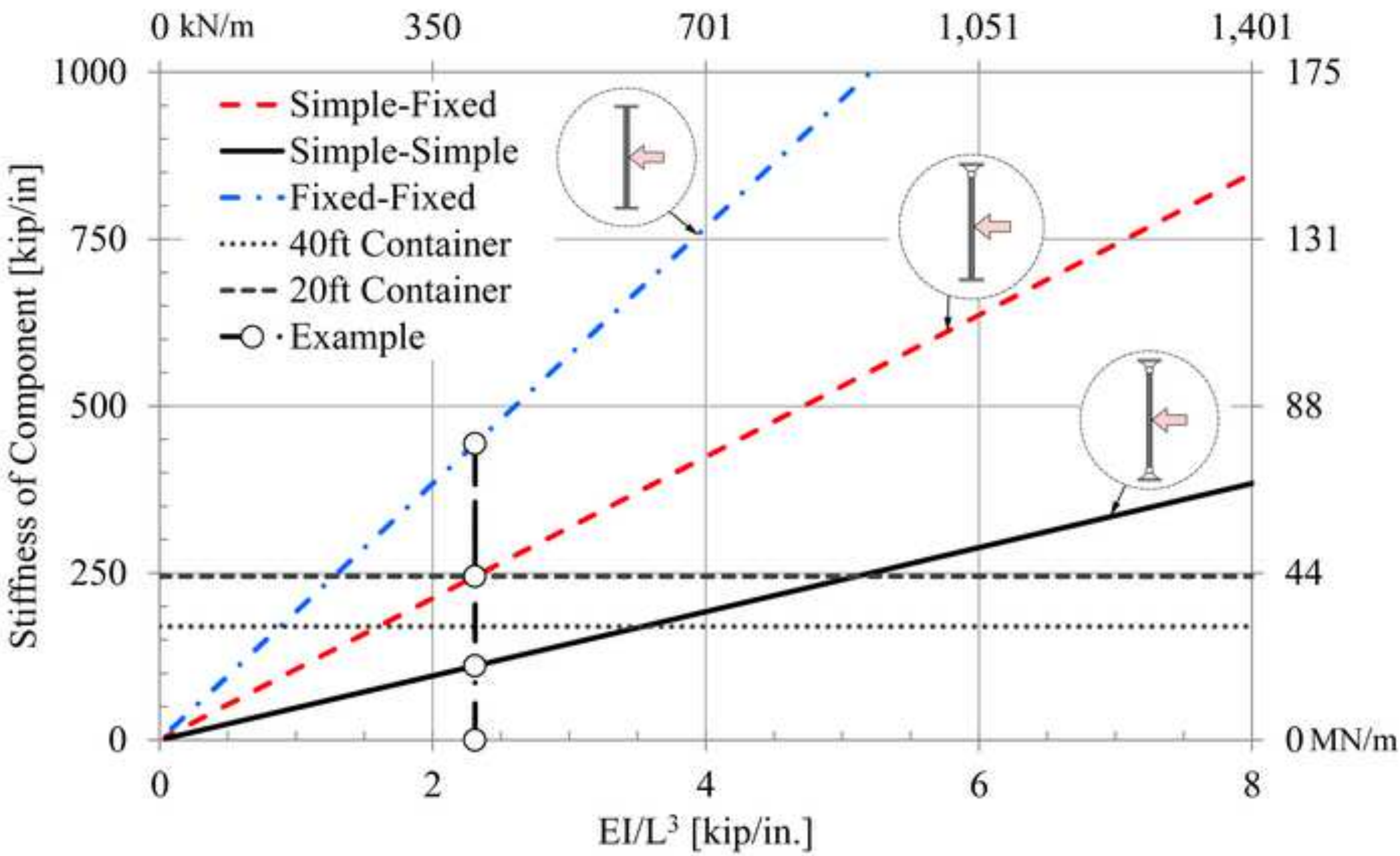

Figure 10. Maximum inundation depth (a) and flow velocity

Click here to download Figure Figure10a.tif

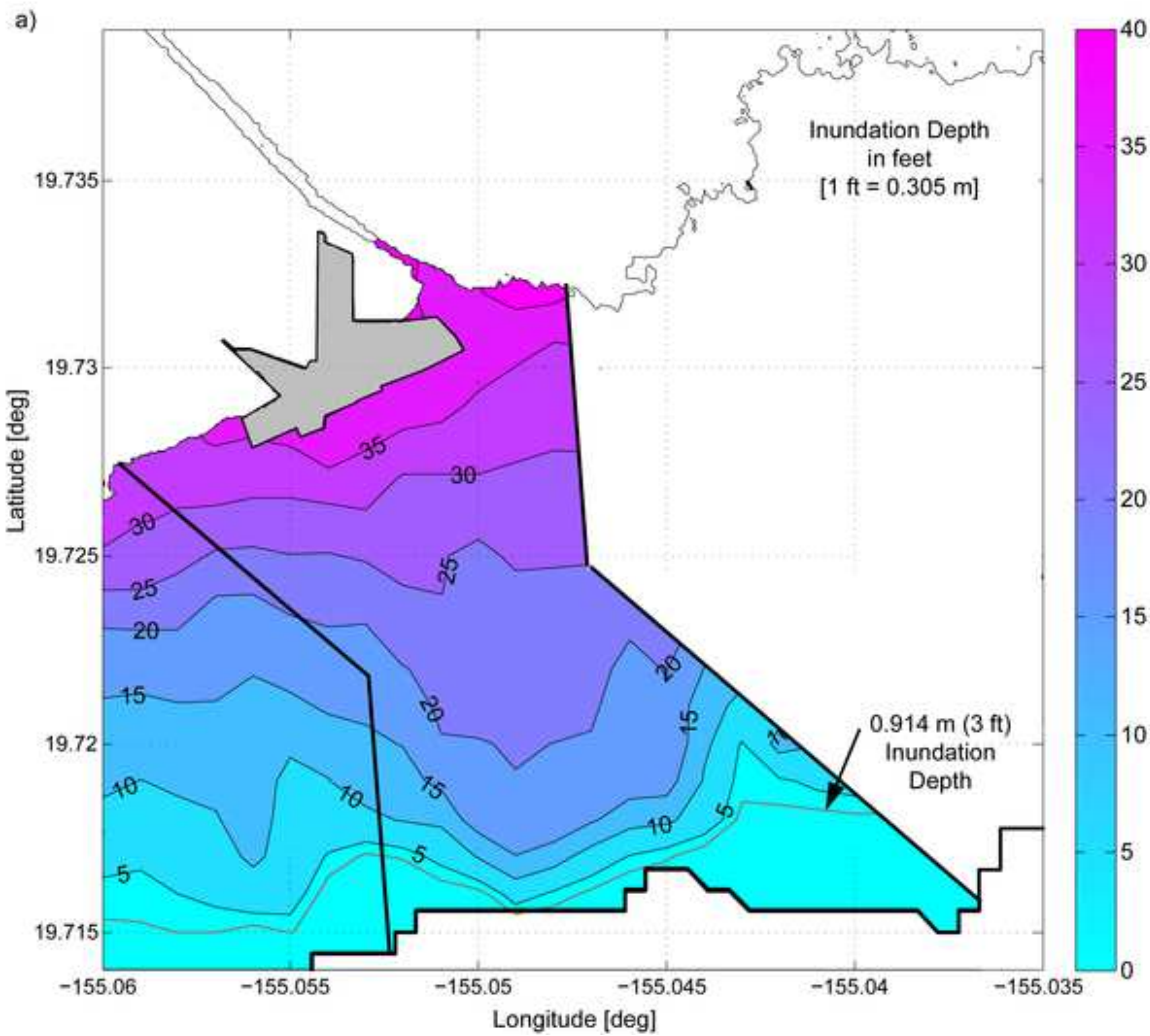

Figure 10. Maximum inundation depth (b) in container impact hazard region

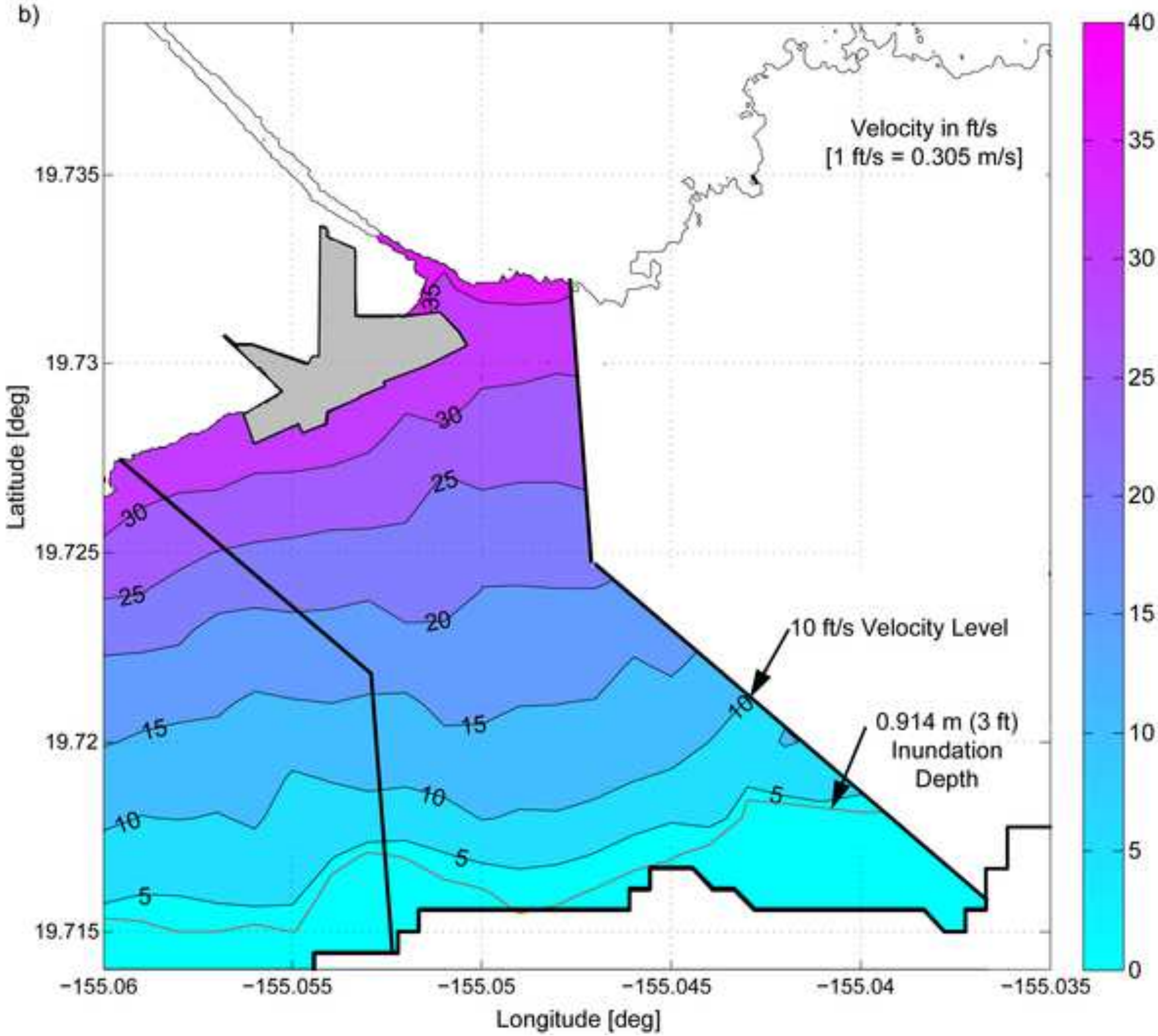

Figure 11. Design instantaneous debris impact force for 6.1 m (20 ft) containers in hazard region for Load Case 2 (a)

Click here to download Figure Figure11a.tif

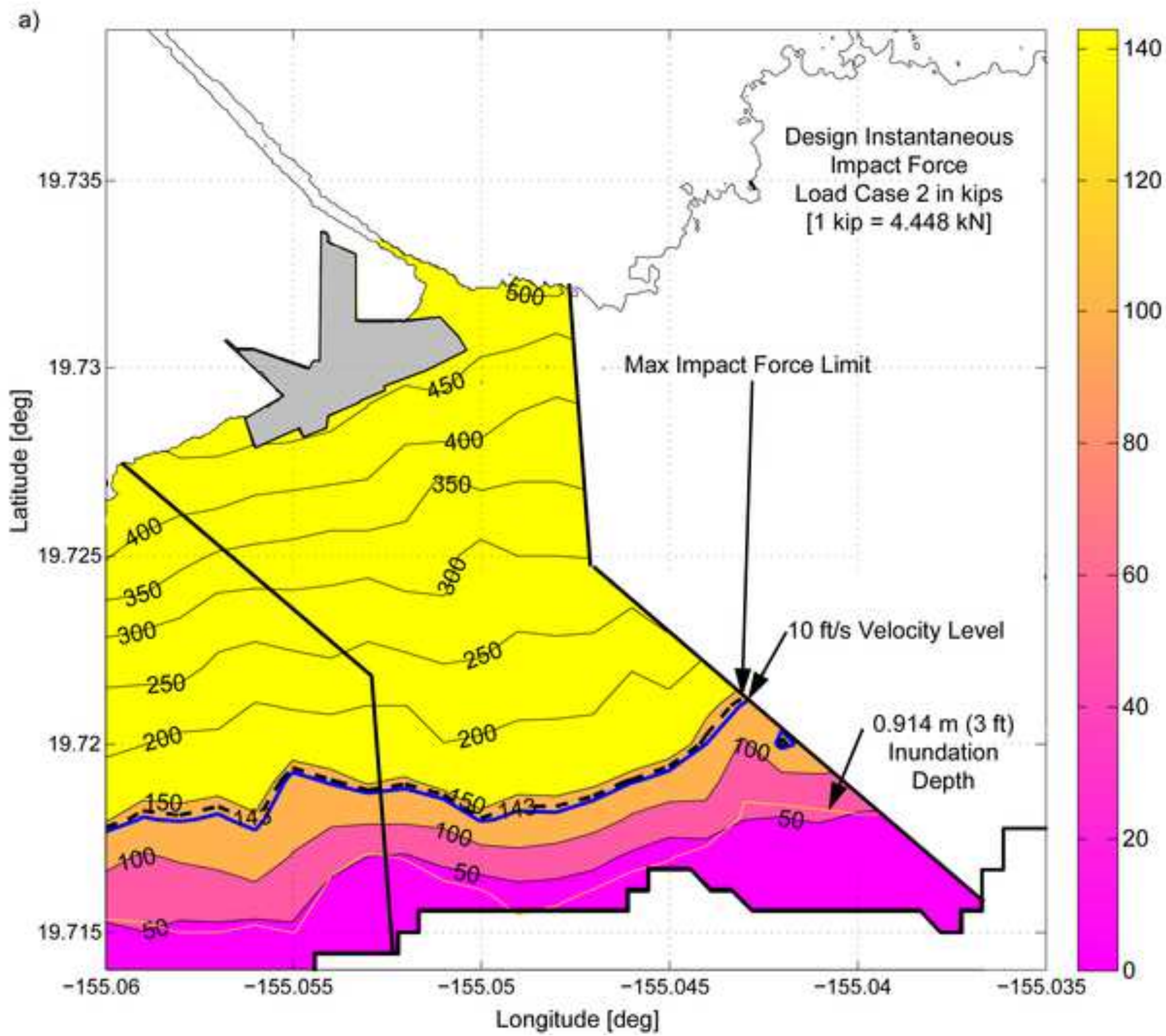

Figure 11. Design instantaneous debris impact force for 6.1 m (20 ft) containers in hazard region for Load Case 3 (b)

Click here to download Figure Figure11b.tif